AUTEX Research Journal, Vol. 18, No 3, September 2018, DOI: 10.1515/aut-2018-0002 © AUTEX

DESIGNS OF TEXTILE ANTENNA ARRAYS FOR SMART CLOTHING APPLICATIONS

Kuo-Sheng Chin[1], Chi-Sheng Wu[1], Chien-Lung Shen[2], Kun-Chuan Tsai[2]

[1]Department of Electronic Engineering, Chang Gung University
No. 259 Wenhwa 1st Rd., Kweishan Dist., Taoyuan, Taiwan, R.O.C.
kschin@mail.cgu.edu.tw; ericannie23@yahoo.com.tw
[2]Taiwan Textile Research Institute
No. 6, Chengtian Rd., Tucheng Dist., New Taipei City, Taiwan, R.O.C.
clShen.0865@ttri.org.tw; kctsai.0815@ttri.org.tw

Abstract:

In this work, three designs of textile antennas, namely, a rectangular microstrip patch antenna, annular slot antenna, and planar inverted-F antenna (PIFA), operating in the 2.45 GHz WLAN band were developed for smart clothing applications. Conductive textile, a copper-plated polyester fabric, was used for fabricating antenna radiators and grounds. An insulating neoprene fabric with a thickness of 4 mm and a permittivity of 1.5 was used for preparing the substrates. The textile patch antenna achieved a maximum gain of 5.96 dBi and a bandwidth of 4.6%. The annual slot antenna showed a moderate gain and bandwidth of 2.9 dBi and 13.1%, respectively. The PIFA achieved the widest bandwidth of 31% but the smallest gain of 1.2 dBi. Furthermore, the performance deterioration of the proposed antennas under various bending conditions was analyzed to evaluate their suitability for wearable applications. Moreover, two 2 × 2 patch and slot antenna arrays were assembled to increase gain and bandwidth. The measured results proved that the developed antenna designs provide superior performance.

Keywords:

Smart clothing, textile antenna, patch antenna, planar inverted-F antenna, slot antenna

1. Introduction

Research on body-centric wireless communication and wearable devices has rapidly increased in recent years because of the various applications of such devices in personal communication systems. Smart clothing (Figure 1) is a wearable personal communication system that can be useful in eldercare, medical emergencies, firefighting, military applications, and athlete monitoring [1]. Conventionally, antennas are fabricated using printed circuit boards (PCBs), which are not flexible, uncomfortable for the human body, and not washable. In addition, the antennas of portable devices provide very limited design space, which imposes performance restrictions. Commercially available products from metalized fabric were Flectron, Shieldex, REMP, Shintron, and so on. Textile antennas with metalized fabric are flexible for raising amenity, are washable, and can be assembled in array configurations to enhance gain. In [2], the recent types of textile antennas were investigated, including suitable material selection, fabrication methods, and analysis required for a wearable antenna design. A high-strength textile suitable for military antenna applications was studied in [3], in which permittivity and the loss tangent were measured under various temperature and humidity conditions. In [4], a circular patch antenna for operation in the WLAN band was designed using a substrate made of an indigo blue jeans cotton fabric. Moreover, rectangular patch antennas prepared using taffeta and polyester were developed for operation in the WLAN band [5]. Performance variations were evaluated under various bending conditions. In [6], patch-type radiofrequency identification tag antennas for use in the UHF band were fabricated using electrotextiles. A structure for a planar inverted-F antenna (PIFA)-type textile antenna was proposed in [7] for increasing bandwidth and preventing frequency shift when the antenna approaches a human body. Pure copper polyester taffeta and ShieldIt were used for fabricating radiators, and a 6-mm fleece fabric was used for preparing the substrate. In [8], a UWB wearable antenna was designed using liquid crystal polymer substrates with superior performance in return loss and radiation pattern under folding, heating, and wetting conditions. In [9], a three-element antenna array driven by a dipole was developed using varactors to control adjacent parasitic element antennas. This antenna array achieved a horizontal sweeping angle of 95° with a peak gain of 6.9 dBi. In [10], a dual-band button antenna with high rigidity was designed for use at 2.4 and 5 GHz; the radiation pattern of this antenna was similar to those of monopole antennas. Another dual-band textile antenna was proposed in [11]; this antenna was loaded with an artificial magnetic conductor (AMC) plane and was fabricated using a rectangular patch and patch-etched slot dipole. The AMC was designed to reduce the substrate thickness and suppress back radiation considerably. Recently, substrate-integrated waveguide (SIW) textile antennas and other wearable circuits constructed using copper tube eyelets were developed [12-15]. SIW-on-textile integration results in an antenna exhibiting high robustness against bending, a low influence on the human body, and a high front-to-back ratio. In [16,17], coupling effects caused by the human body position on textile antennas were studied. The chest showed the greatest effect, with a pattern average difference of 24%.

This paper systematically describes the design of textile antennas for smart clothing applications including the analysis of electrical characteristics of substrates, fabrication process, comparison of three typical antenna structures, performance degradation under bent conditions, and the integration of antenna array. Three textile antennas, namely, rectangular patch, annular slot, and PIFA, operating in the 2.45-GHz WLAN band were developed. Furthermore, two 2 × 2 patch and slot antenna arrays were assembled for achieving high gain.

2. Material Characteristics of Textiles

Metallic radiators and ground planes are required for constructing antennas. Conventionally, conductive textiles are often chosen to fabricate radiators for textile antennas because of their low sheet resistance (<1 W/□). Furthermore, insulating fabrics are often chosen to prepare substrates for supporting radiators; these fabrics typically have a permittivity of 1.5−3.29, a loss tangent of 0.0004−0.04, and a thickness of 0.125−6 mm [2,3].

2.1. Conductive Textile and Neoprene Substrate

Figure 2 shows typical conductive textiles prepared using metal strands, printed, and coated with electrically conductive materials. In this work, a conductive textile with a copper-plated polyester fabric developed by Formosa Taffeta Co., Ltd. (product number: FCN-M451A) was applied for constructing the radiator and ground of antennas. Table 1 lists the surface resistances of the proposed conductive textiles after wet-heating and salt-spraying tests, with the textiles achieving a superior sheet resistance of <0.08 W/□. Synthetic-rubber-containing insulating neoprene substrates provided by Taiwan Textile Research Institute (TTRI), which possessed superior wrinkle, stretching, and bending resistance, was used to support the radiator and ground plane. Figure 3 shows the photographs of the conductive textile and neoprene substrate.

2.2. Heat-Press Laminating Process

A laser carving machine was used for cutting the conductive textile to the desired shape with high accuracy. The cut-out pieces of the conductive textile and neoprene substrate were joined together to construct the antenna structure. For this, the cost-effective heat-press laminating process was adopted, in which a thermoplastic polyurethane film was used for fabric adhering. The setting conditions for the heat-press laminator were 130°C and 13 s. Figure 4 shows the photographs of the laser carving machine and heat-press laminator.

2.3. Permittivity of Neoprene Substrate

The relative permittivity of the neoprene substrate (thickness, 4 mm) was measured using the resonant-ring method. In this method, the ring resonates at its fundamental frequency when its median circumference equals one guided wavelength. Three resonant rings with different diameters for operation at 0.84, 1.65, and 4.03 GHz to completely cover the required microwave band were designed on the neoprene substrate. Table 2 lists the measured relative permittivity (εr) values of the neoprene substrate with an average εr value of 1.5; here $\varepsilon reff$ denotes the effective permittivity.

3. Design of Textile Antennas

This work compares three types of textile antennas—a patch antenna, slot antenna, and PIFA—all operated at 2.45 GHz.

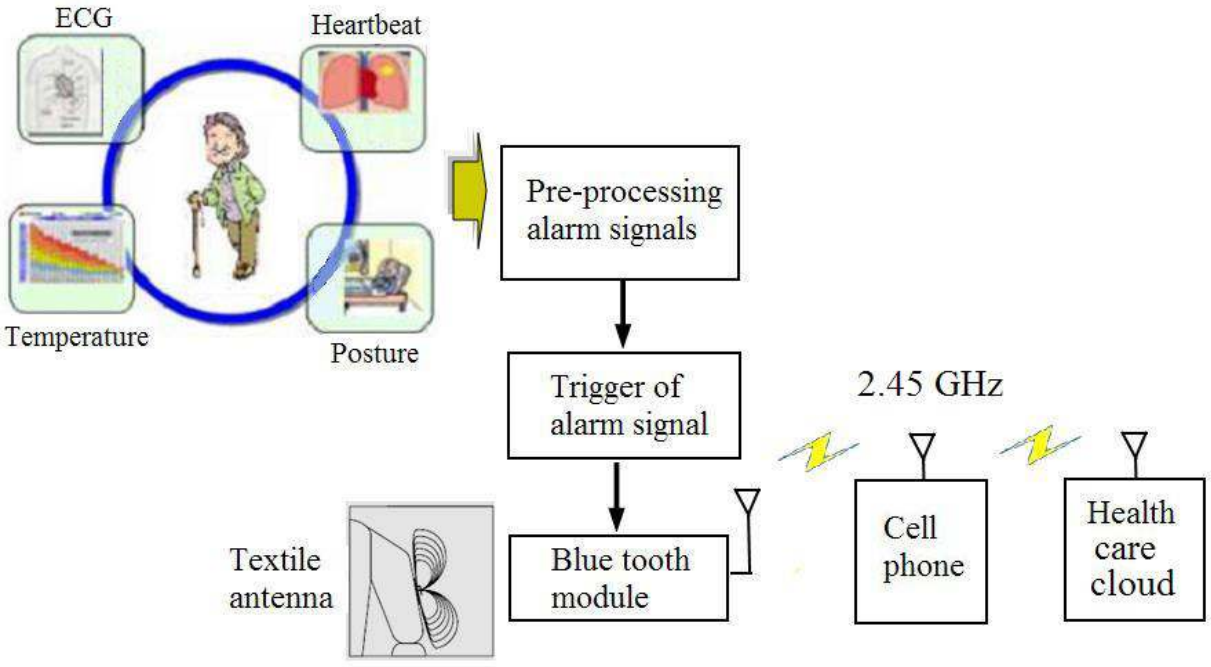

Figure 1. Textile antennas for smart clothing applications.

(a)

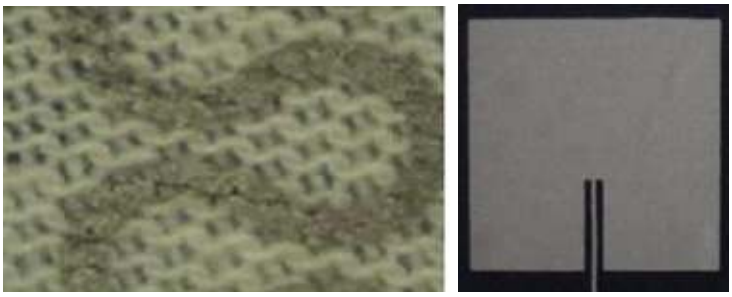

(b)

Figure 2. Typical conductive textiles: (a) embedded with metal strands and (b) printed or coated with electrically conductive materials.

Table 1. Surface resistance of proposed conductive textiles

Surface resistance on first Stage	Warp	Ω/□	0.05↓
	Weft	Ω/□	0.05↓
After wet-heating test	Warp	Ω/□	0.07↓
	Weft	Ω/□	0.07↓
After salt-spraying test	Warp	Ω/□	0.08↓
	Weft	Ω/□	0.08↓

(a) (b)

Figure 3. Photographs of (a) conductive textile and (b) neoprene substrate.

(a) (b)

Figure 4. Photographs of (a) laser carving machine and (b) heat-press laminator.

3.1. Design of Textile Patch Antenna

Figure 5 shows the structure of the textile rectangular patch antenna and smart clothing, in which the white and black areas are the conductive textile and neoprene substrate, respectively. The patch antenna consists of a conductive patch attached on the top of neoprene substrate with a ground plane on the bottom of the substrate. When the length of patch is approximately $\lambda g/2$, where λg is the guided wavelength, the patch becomes resonant and the electromagnetic field can be radiated. The resonant length of the patch in the TM_{10} mode was 46.5 mm, and a microstrip inset feed line was used for signal excitation. The input impedance of the patch antenna at 186 Ω was transformed to 50 Ω by using a $\lambda g/4$ impedance transformer. Table 3 lists the dimensions of the textile patch antenna.

3.2. Design of Textile Slot Antenna

Figure 6 shows the proposed textile slot antenna in which the annular slot appears as a black ring. The annular slot antenna consists of a circular slot on a square, conductive ground plane that was fed by a microstrip line, fabricated on the bottom of the neoprene substrate. The mean length of the slot circumference is approximately λg at the design frequency. The annular slot acts as a radiator with excitation current around the periphery of the slot. The black strips in Figure 6(b) are Velcro strips installed for fixing the antenna to the smart clothing for testing. Because the substrate is thick, the feed line impedance of 50 Ω requires a line width of 16.5 mm, which may result in undesired transverse resonance and high-order modes. Therefore, the feed line was designed to have a high impedance of 187 Ω,

Table 2. Measured permittivity of neoprene substrates

	f_0 (GHz)	ε_{reff}	ε_r
Ring 1	4.03	1.35	1.56
Ring 2	1.65	1.25	1.41
Ring 3	0.84	1.43	1.65

Table 3. Dimensions of textile patch antenna

Length of patch	46.5 mm	**Length of ground**	110 mm
Width of patch	50 mm	**Width of ground**	110 mm
Length of $\lambda g/4$ transformer	25 mm	**Depth of inset feed**	7 mm
Width of $\lambda g/4$ transformer	5.5 mm	**Width of inset feed**	1 mm

Figure 5. Fabricated textile patch antenna and smart clothing.

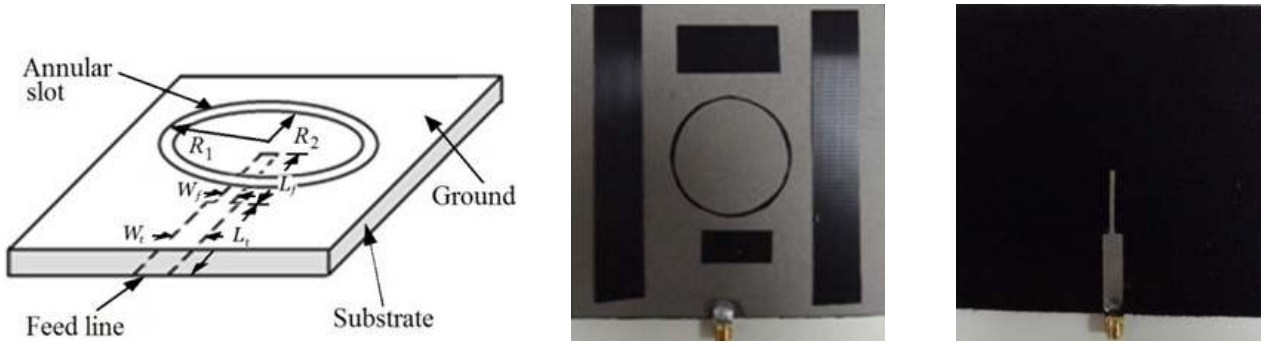

(a) (b) (c)

Figure 6. Textile annular slot antenna: (a) 3D schematic view, (b) top view, and (c) bottom view.

corresponding to a line width of 1 mm. A λ*g*/4 transformer with an impedance of 96 Ω and a line width of 5.5 mm was used for impedance matching. Table 4 lists the dimensions of the textile annular slot antenna.

3.3. Design of Textile PIFA

Figure 7(a) shows a 3D schematic of the proposed textile PIFA. The PIFA consists of main radiating patch, a rectangular ground plane, a shorted plate, and a coaxial feed. PIFA can be considered as a kind of linear inverted-F antenna (IFA) with the wire radiator element replaced by a plate to expand the bandwidth. The resonant frequency of the PIFA increases with a decrease in *h* or an increase in either *D* or *W*. When *W* equals L_2, L_1 is approximately equal to λ*g*/4. Figure 7(b) and 7(c) shows the photographs of the proposed textile PIFA with an SMA connector. The resonant frequency increases with *W*, whereas the depth of S_{11} decreases. Table 5 lists the dimensions of the textile PIFA.

Table 5. Dimensions of textile PIFA

Design parameter	Dimension	Design parameter	Dimension
L_1	19 mm	*Lw*	19 mm
L_2	19 mm	*Ll*	50 mm
W	4 mm	*D* 15 mm	
h	4 mm		

4. Design of Two 2 × 2 Textile Antenna Arrays

Two antenna arrays consisting of 2 × 2 patch and slot elements were designed to achieve high gain and a wide bandwidth for smart clothing applications.

Table 4. Dimensions of textile annular slot antenna

R_1	**19 mm**	**Width of slot**	**1 mm**
R_2	18 mm	*Lt*	25 mm
Lf	24 mm	*Wt*	5.5 mm
Wf	1 mm	Ground plane 98 × 98 mm²	

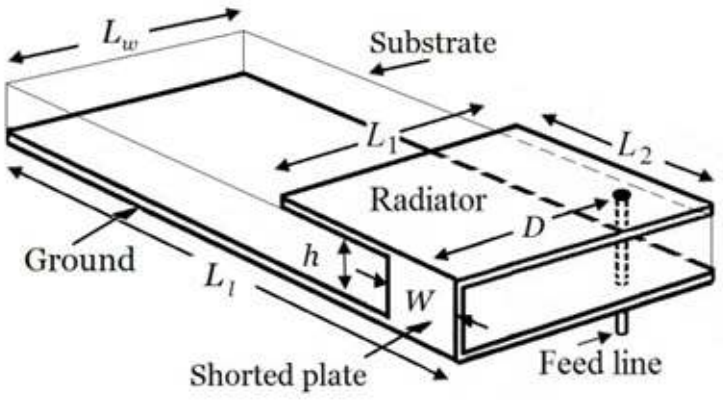

(a)

(b)

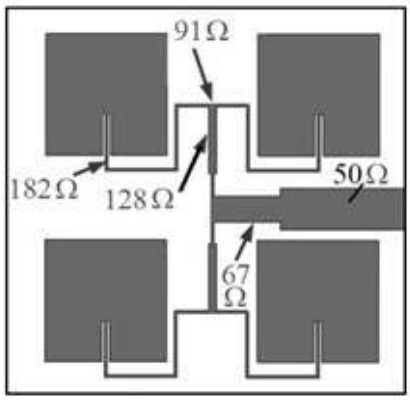

(c)

Figure 7. Textile PIFA: (a) 3D schematic view, (b) top view, and (c) bottom view.

4.1. 2×2 Textile Patch Antenna Array

The integration of the 2 × 2 patch antenna elements is depicted in Figure 8, which shows a photograph of the fabricated array and the impedance arrangement of the feeding network. The patch element had a length of 46.5 mm and a width of 50 mm and was operated at 2.45 GHz. The feeding network was designed with a minimum line width of 1 mm to obey the design rule of the finishing process, which corresponded to an impedance of 182 Ω. The 2D parallel inset feeding network was composed of power dividers and impedance transformers with five impedances of 182, 128, 91, 67, and 50 Ω.

4.2. 2×2 Textile Annular Slot Antenna Array

Figure 9(a) and 9(b) shows the photographs of another fabricated 2 × 2 textile annular slot antenna array. The slot elements had a median radius of 18.5 mm and a gap of 1 mm. A microstrip parallel feeding network with four impedances of 182, 128, 91, and 67 Ω was designed. Figure 9(c) shows the impedance arrangement of the feeding network.

5. Measured Results and Comparison

For demonstrating the effectiveness of the proposed textile antenna designs, five experimental textile antennas—three single antennas and two antenna arrays—were fabricated.

5.1. Textile Patch Antenna

Figure 10 shows the simulated and measured S_{11} responses of the experimental textile patch antenna, which are in good agreement. The measured center frequency was 2.56 GHz with a 10-dB impedance bandwidth of 4.6%. Figure 10(b) and 10(c) shows plots for the E- and H-plane radiation patterns at

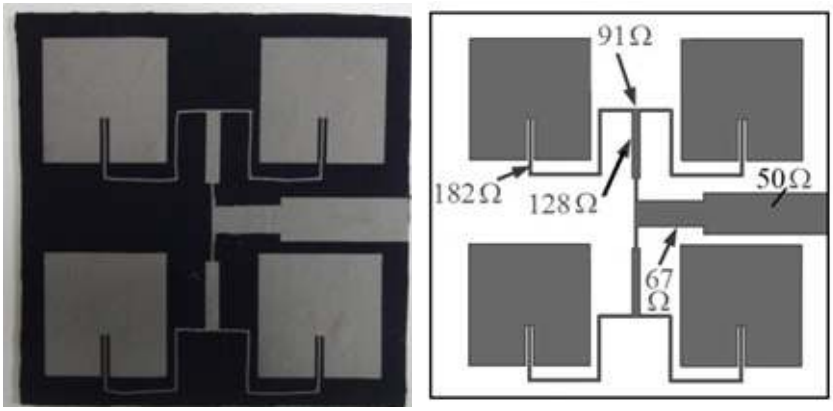

Figure 8. Fabricated 2 × 2 textile patch antenna array with impedance arrangement of feeding network.

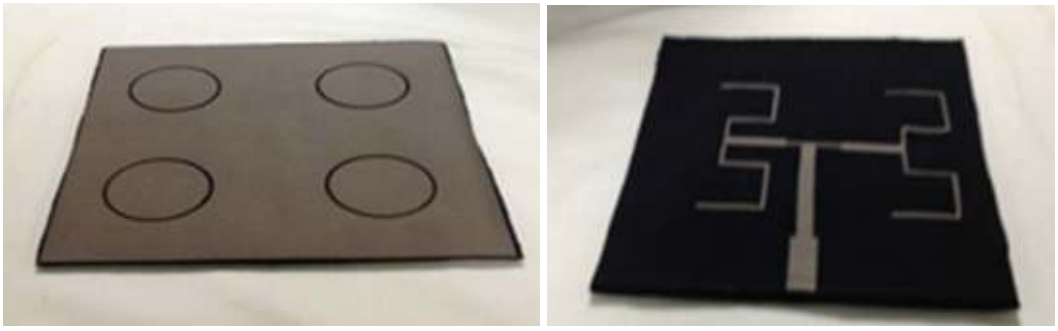

(a) (b)

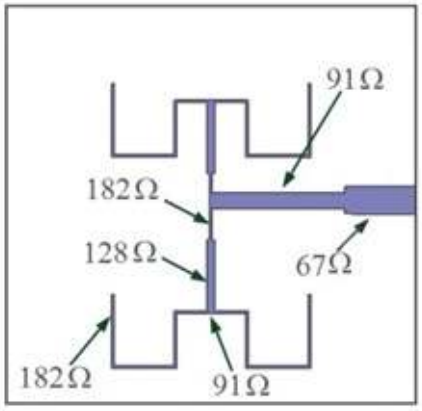

(c)

Figure 9. Fabricated 2 × 2 textile annular slot antenna array: (a) front view and (b) rear view. (c) Impedance arrangement of the feeding network.

2.56 GHz, respectively. The simulated and measured maximal gains were 7.34 and 5.96 dBi, respectively. Because of the shielding effect of the ground plane, the signal strength of back radiation decreased significantly.

5.2. Textile Annular Slot Antenna

Figure 11 shows the simulated and measured S_{11} responses and radiation patterns of the textile annular slot antenna. The measured center frequency was 2.25 GHz with a bandwidth of 13.1% (simulated result, 12.5%), which is higher than that of the patch antenna. Figure 11(b) and 11(c) presents the radiation patterns at 2.25 GHz. The simulated and measured maximal gains were 4.4 and 2.9 dBi, respectively. The reduced gain may be attributed to the fabrication tolerance. The signal strength of back radiation was similar to that of front radiation because the slot could radiate on both sides of the ground.

5.3. Textile PIFA

Figure 12(a) shows the S_{11} parameter responses of the textile PIFA. The parameter W was chosen to be 4 mm for resonance at 2.45 GHz with an S_{11} depth of −30 dB. The simulated and measured bandwidths were 28% and 31%, respectively. The measured center frequency was 2.63 GHz. Figure 12(b) and 12(c) shows plots for the E- and H-plane radiation patterns, respectively. The measured peak gain was 1.2 dBi (simulated result, 1.78 dBi). The patterns showed small ripples because of reflection caused by the SMA connector and connection cables used in the test.

Table 6 shows a performance comparison of the three textile antennas. As indicated, the patch antenna showed the highest measured gain of 5.96 dBi because of its largest effective aperture. Second advantage of patch antenna is having reduced backward radiation toward the user's body; this is conducive for reducing the specific absorption rate (SAR) on the human body. However, the patch antenna has the smallest bandwidth of 4.6% because of its resonant nature. The PIFA showed the widest bandwidth of 31%, but the lowest gain of 1.2 dBi. As mentioned, PIFA is a kind of linear IFA with the wire radiator element replaced by a plate to expand the bandwidth. The proposed PIFA exhibits omnidirectional H-plane patterns, which is very useful for body-centric wireless communication. Compared with the other antennas, the slot antenna showed a moderate gain and bandwidth. Slot antenna possesses high backward radiation, which may raise SAR. If dimensions are of most concern, the PIFA had the smallest circuit dimensions of

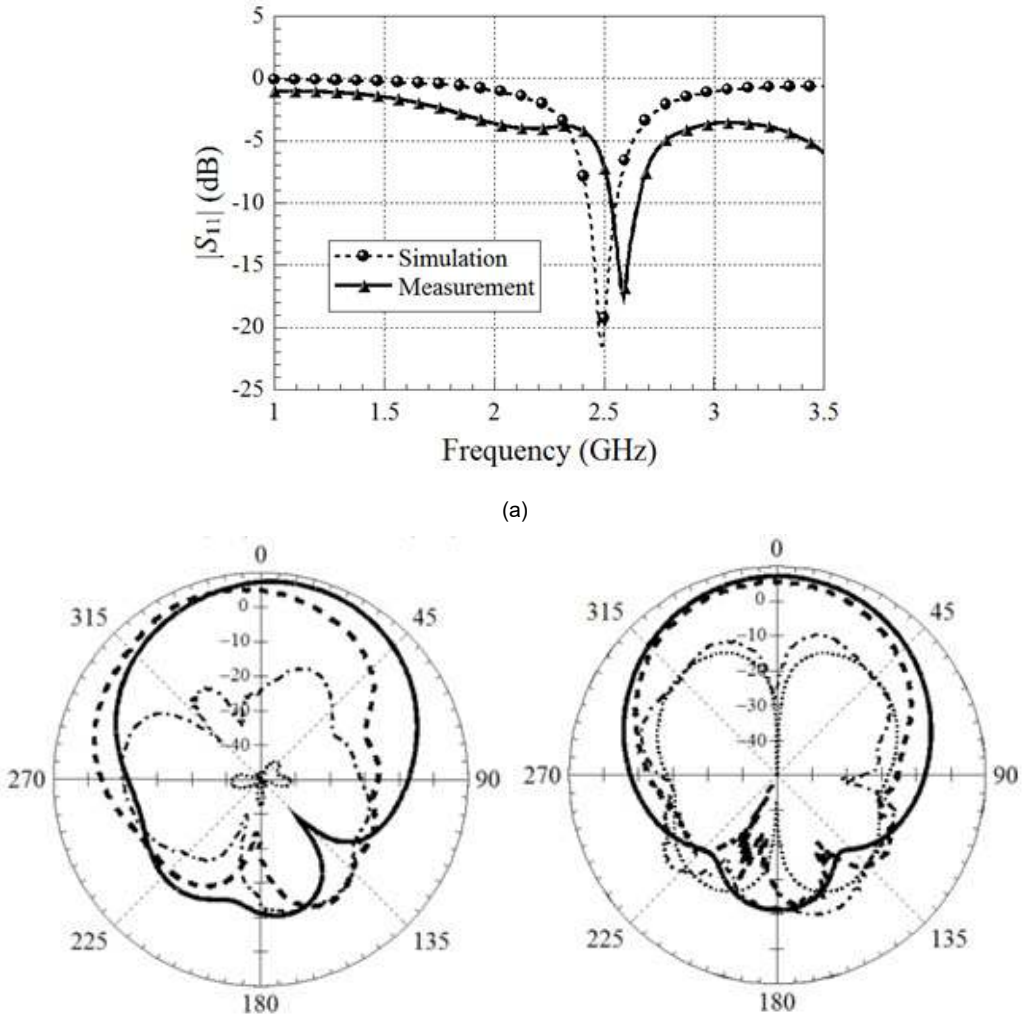

Figure 10. Measured results for textile patch antenna: (a) S_{11} responses, (b) E-plane patterns, and (c) H-plane patterns.

1.9 × 5 cm^2, whereas the patch and slot antennas had larger dimensions of 11 × 11 cm^2 and 9.8 × 9.8 cm^2, respectively.

5.4 Analysis of Bending Effects

Performance deterioration of the proposed textile antennas under various bending conditions was analyzed for evaluating their compatibility for wearable applications. Styrofoam cylinders with different radii provide the desired curvature for the analysis of bending effects. The arc length was fixed to be $S = R \times \theta$, where R is the radius and θ is the angle between the two lateral sides of the antennas as shown in Figure 13(a). Five radii of R = 5, 7, 10, 13, and ∞ (flat case) (all values in cm) were used to define the bending curvature, with a fixed S of 11 cm. Figure 13(b) shows a photograph of the bending textile patch antenna fixed on a Styrofoam cylinder.

Figure 14 shows the measured S_{11} responses of the textile patch antenna under various bending conditions. The depth of S_{11} increased as the curvature decreased. The center frequency remained unchanged because of the bending direction along the nonradiation edge, which reduced the bending effects considerably. Figure 15(a) and 15(b) shows the radiation patterns of the textile patch antenna with R = 5

Table 6. Performance comparison of three textile antennas

Performance		Patch	Slot	PIFA
Gain (dBi)	simulated	7.34	4.4	1.78
	measured	5.96	2.9	1.2
Measured center frequency (GHz)		2.56	2.25	2.63
Measured bandwidth (%)		4.6 13.1		31
Circuit size (cm^2)		11 × 11	9.8 × 9.8	1.9 × 5

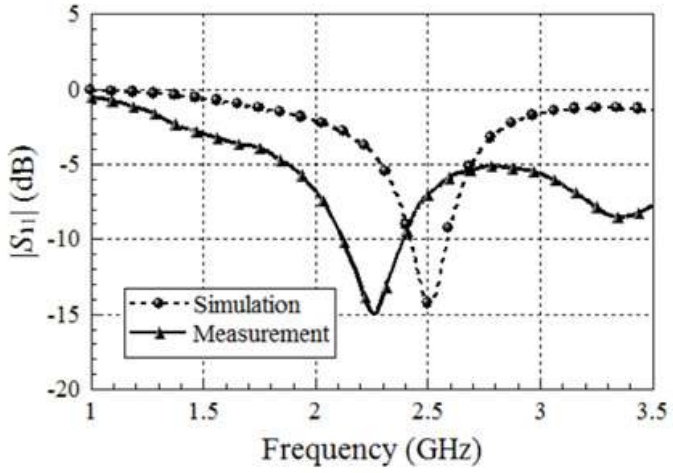

(a)

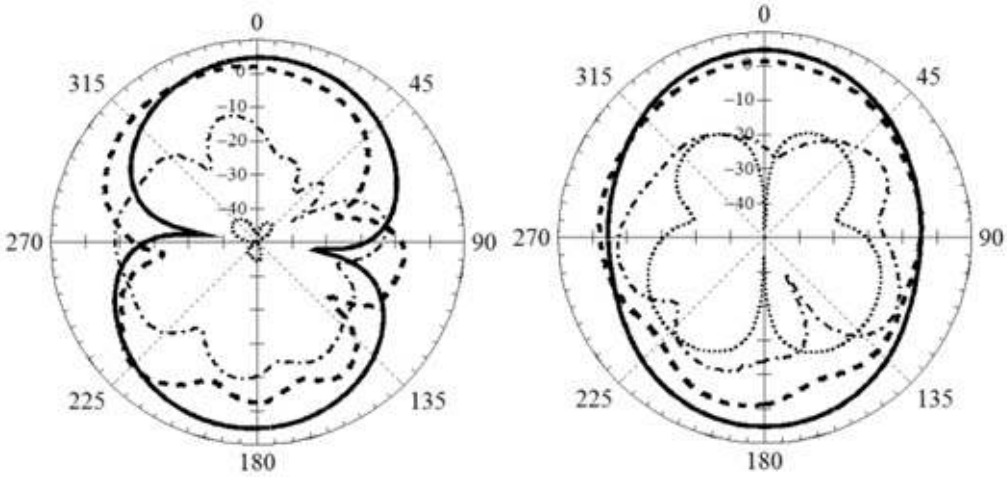

(b) (c)

Figure 11. Measured results for textile annular slot antenna: (a) S_{11} responses, (b) E-plane patterns, and (c) H-plane patterns. Co-Pol. (sim.) Co-Pol. (mea.) Cross-Pol. (sim.) Cross-Pol. (mea.)

cm. Compared with the flat case shown in Figure 10, only a minor variation was observed. The measured gain was 5.37 dBi, which is less than the flat case value of 5.96 dBi by 0.59 dB. Figure 15(c) and 15(d) shows the radiation patterns of the textile patch antenna with R = 10 cm. The results are similar to those for the case with R = 5 cm. Table 7 lists analysis results for bending effects on the patch antenna. As indicated, the center frequency remained almost constant, whereas the bandwidth decreased slightly with increasing curvature. Table 8 lists analysis results for bending effects on the slot antenna; the results are similar to those for the patch antenna.

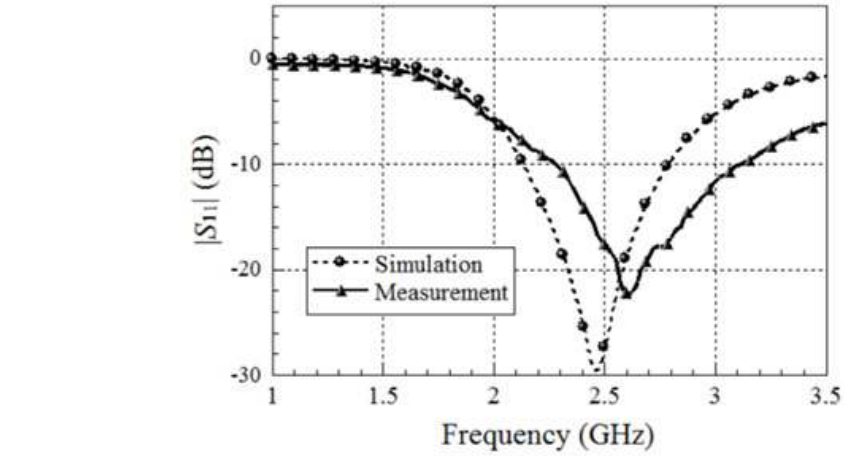

(a)

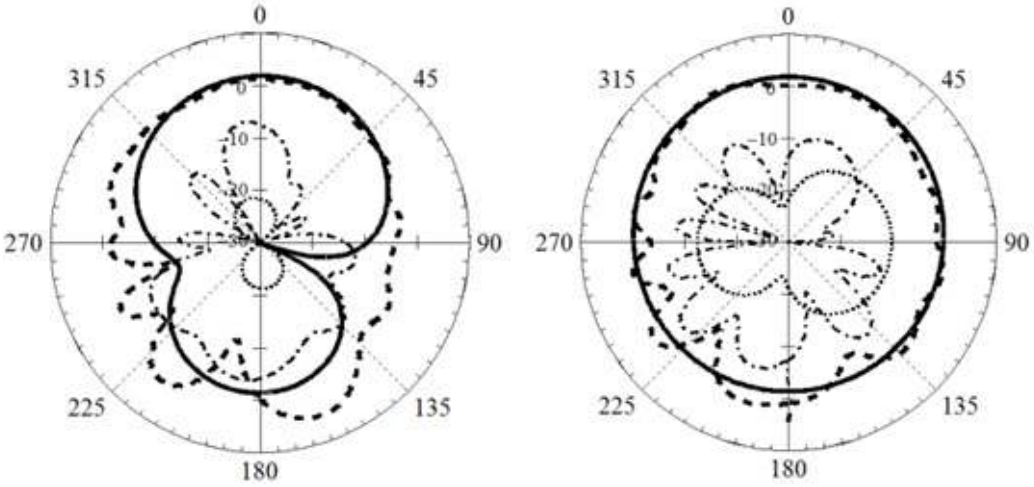

(b) (c)

Figure 12. Measured results for textile PIFA: (a) S_{11} responses, (b) E-plane patterns, and (c) H-plane patterns.

Co-Pol. (sim.) Co-Pol. (mea.) Cross-Pol. (sim.) Cross-Pol. (mea.)

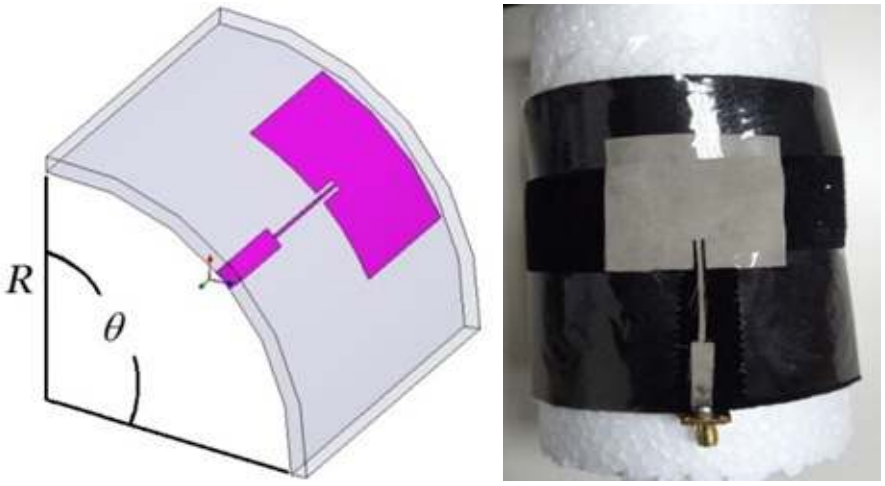

(a) (b)

Figure 13. (a) Definition of bending conditions. (b) Photograph of bending textile patch antenna.

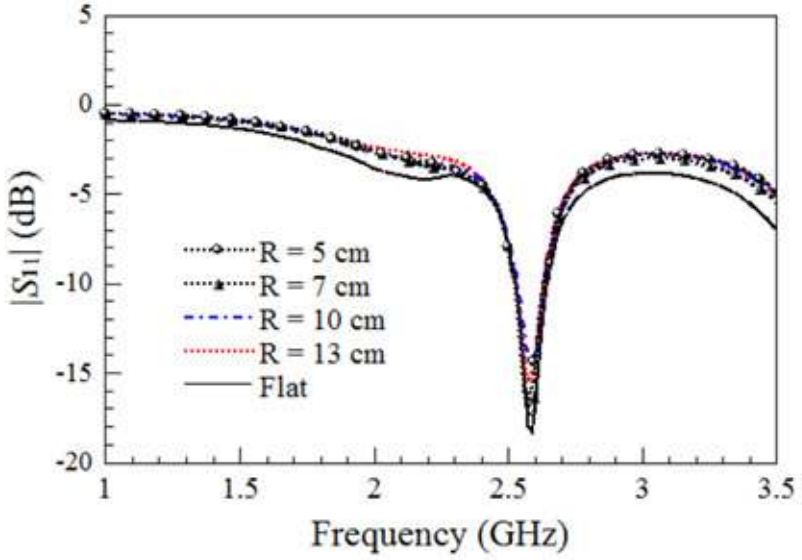

Figure 14. Measured S_{11} responses of textile patch antenna under various bending conditions.

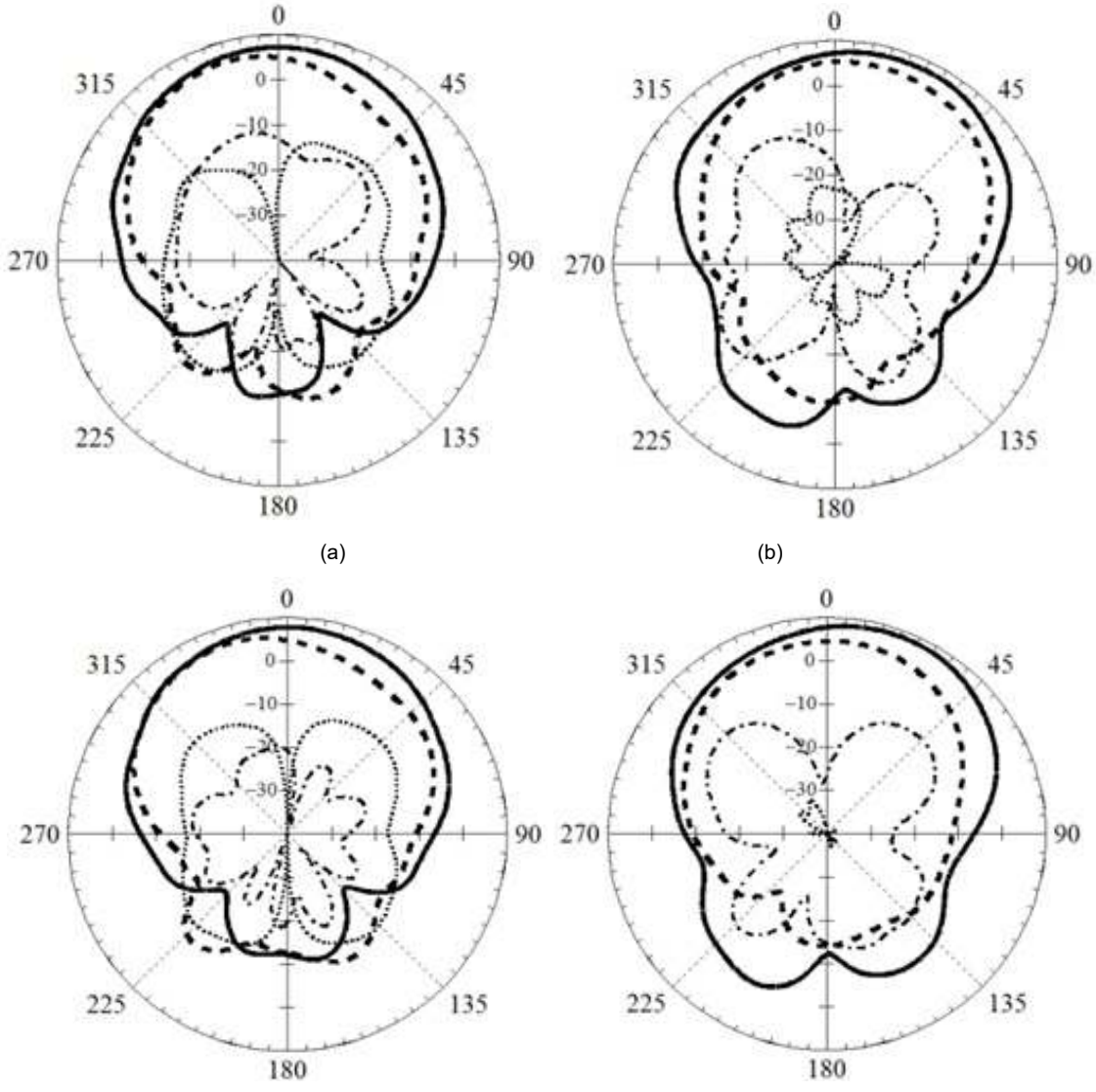

Figure 15. Patch antenna with R = 5 cm, (a) E-plane and (b) H-plane patterns, and with R = 10 cm, (c) E-plane and (d) H-plane patterns.
Co-Pol. (sim.) Co-Pol. (mea.) Cross-Pol. (sim.) Cross-Pol. (mea.)

5.5. 2 × 2 Textile Patch Antenna Array

Figure 16(a) shows the measured and simulated S_{11} responses of the 2 × 2 patch antenna array. The measured center frequency was 2.43 GHz with a bandwidth of 10%. Notably, an extra resonance occurred at 3.16 GHz. This additional resonance may be attributed to the feed line and SMA connector, which had a line width of 16 mm that may have resulted in a discontinuity.

Figure 16(b) and 16(c) shows the radiation patterns of the patch antenna array at 2.43 GHz. Expectedly, front radiation was reinforced. The measured maximal gain was 8.06 dBi, which is 2.1 dB higher than that of the single patch antenna. The deviation from an array factor of 6 dB was mainly caused by the heavy loss of 3.9 dB in the feeding network. Because the proposed antenna array was symmetrically fed, the symmetry of the radiation patterns was preserved.

Table 7. Bending effects on textile patch antenna

Bending conditions	Bending radius (cm)				
	R = 5	*R* = 7	*R* = 10	*R* = 13	Flat
Center freq. (GHz)	2.57	2.58	2.58	2.57	2.56
Bandwidth (%)	3.96	4.3	4.14	4.12	4.6

Table 8. Bending effects on textile slot antenna

Bending conditions	Bending radius				
	5 cm	7 cm	10 cm	13 cm	Flat
Resonant freq. (GHz)	2.26	2.26	2.24	2.25	2.25
Bandwidth (%)	12.25	12.41	12.56	12.9	13.1

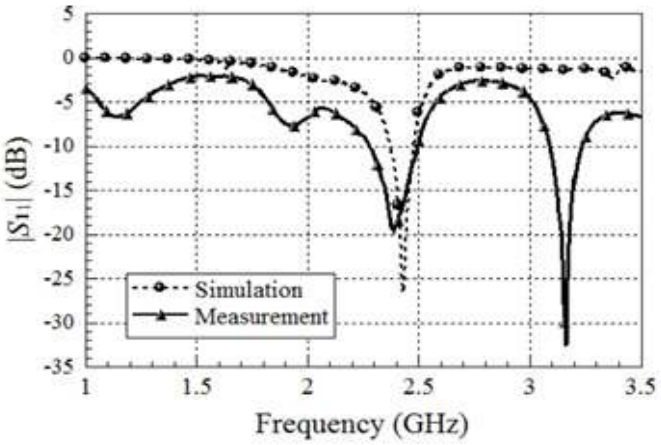

(a)

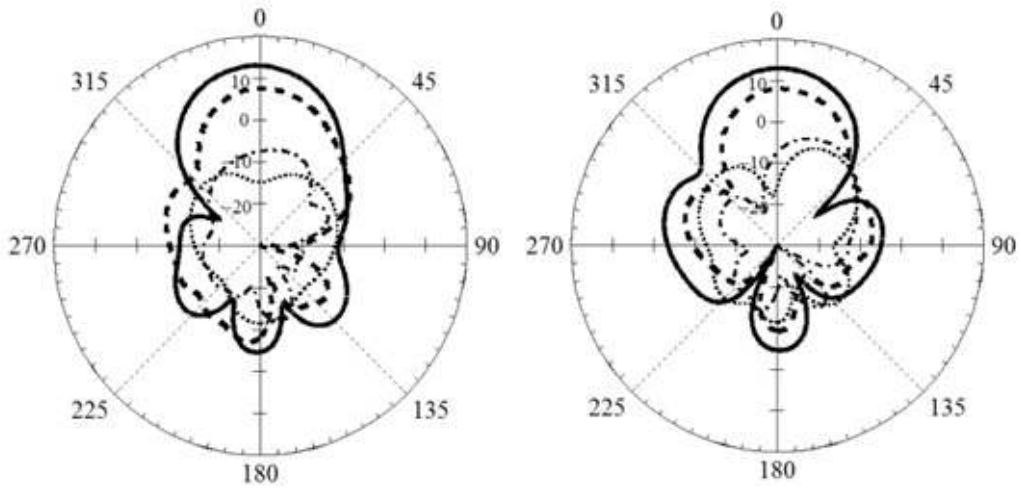

(b) (c)

Figure 16. Radiation patterns of 2 × 2 patch antenna array: (a) S_{11} responses, (b) E-plane patterns, and (c) H-plane patterns.

Co-Pol. (sim.) Co-Pol. (mea.) Cross-Pol. (sim.) Cross-Pol. (mea.)

5.6. 2×2 Textile Annular Slot Antenna Array

Figure 17(a) shows the measured S_{11} responses of the fabricated 2 × 2 slot antenna array with a center frequency of 2.44 GHz and a bandwidth of 12.9%. Similar to the patch antenna array, the slot antenna array showed an extra resonance at 3 GHz. Figure 17(b) and 17(c) shows the E- and H-plane radiation patterns, respectively. The measured maximal gain was 7.16 dBi (simulated result, 8.2 dBi). This gain was 4.26 dB higher than that of the single slot antenna. Therefore, the loss caused by the feed network was 1.74 dB. Both the front and back radiations were reinforced.

6. Conclusions

In this work, three textile antennas operating in the 2.45-GHz WLAN band were developed for smart clothing applications. The systematic design including the analysis of electrical characteristics of substrates, fabrication process, comparison of three typical antenna structures, and performance degradation under bent conditions was presented. Moreover, two 2 × 2 patch and slot antenna arrays were assembled to enhance gain and bandwidth. All measured results show that the proposed antenna designs have superior performance.

ACKNOWLEDGMENTS

This study was partially supported by the Ministry of Science and Technology (MOST 105-2221-E-182-010) and Chang Gung University (BMRP 903), Taiwan, R. O. C.

References

[1] Y. Wang, L. Li, B. Wang, and L. Wang, A body sensor network platform for in-home health monitoring application, Proceedings of the 4th International Conference on Ubiquitous Information Technologies & Applications (2009), 1-5.

[2] N. H. M. Rais, P. J. Soh, F.Malek, S. Ahmad, N.B.M. Hashim, and P.S Hall, A review of wearable antenna, Loughborough Antennas & Propagation Conference, (2009), 225-228.

[3] J. Lilja and P. Salonen, Textile material characterization for softwear antennas, MILCOM'09 Proceedings of the 28th IEEE conference on Military communications, (2009), 628-634.

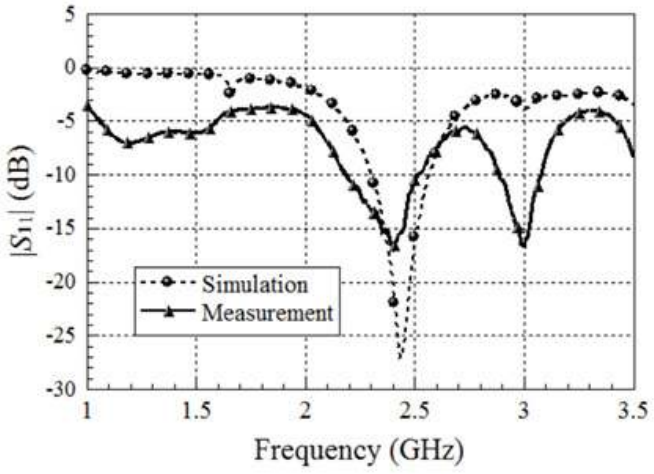

(a)

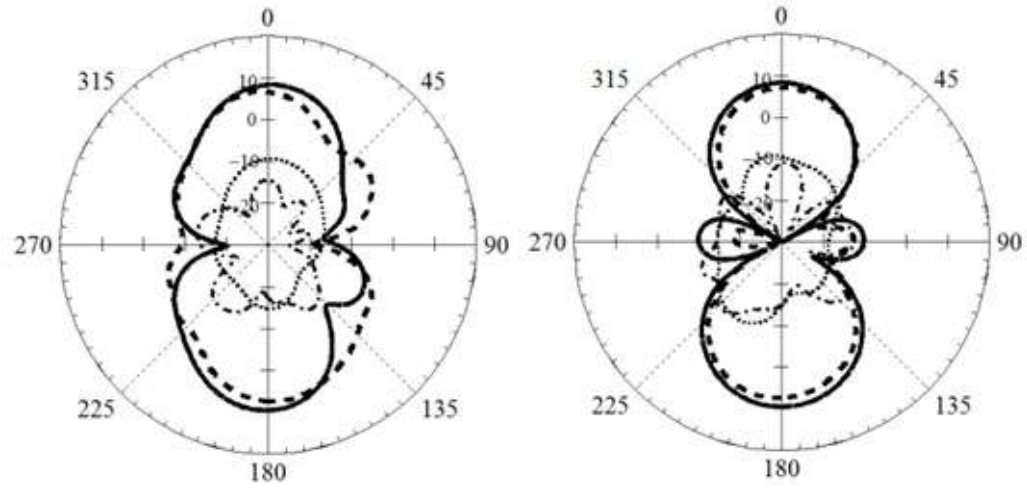

(b) (c)

Figure 17. Measured results for 2 × 2 annular slot antenna array: (a) S_{11} responses, (b) E-plane radiation patterns, and (c) H-plane radiation patterns.

Co-Pol. (sim.) Co-Pol. (mea.) Cross-Pol. (sim.) Cross-Pol. (mea.)

[4] S. Sankaralingam and B. Gupta, A circular disk microstrip WLAN antenna for wearable applications, Annual IEEE India Conference (INDICON), (2009), 1-4.

[5] S. Sankaralingam and B. Gupta, Development of textile antennas for body wearable applications and investigations on their performance under bent conditions, Progress In Electromagnetics Research B, (2010), 22: 53-71.

[6] K. Koski, A. Vena, L. Sydänheimo, L. Ukkonen, and Yahya Rahmat-Samii, Design and implementation of electro-textile ground planes for wearable UHF RFID patch tag antennas, IEEE Antennas Wireless Propagat. Lett., (2013), 12: 964-967.

[7] P. J. Soh, G. A. E Vandenbosch, V. Volski, and H. M. R. Nurul, Characterization of a simple broadband textile planar inverted-F antenna (PIFA) for on body communications, Conference Proceedings ICECom, (2010), 1-4.

[8] M. H. Sagor, Q. H. Abbasi, A. Alomainy, and Y. Hao, Compact and conformal ultra wideband antenna for wearable applications, Proceedings of the 5th European Conference on Antennas and Propagation (EUCAP), (2011),. 2095-2098.

[9] M. R. Islam and M. Ali, A novel wearable antenna array for 2.45 GHz WLAN application, IEEE International Symposium on Antennas and Propagation (APSURSI), (2011), 2754-2757.

[10] B. Sanz-Izquierdo, J. C. Batchelor, and M. I. Sobhy, Button antenna on textiles for wireless local area network on body applications, IET Microw. Antennas Propag., (2010), 4(11): 1980–1987.

[11] S. Yan, P. J. Soh, and G. A. E. Vandenbosch, Low-profile dual-band textile antenna with artificial magnetic conductor plane, IEEE Trans. Antenna Propagat., (2014), 62(12): 6487-6490.

[12] R. Moro, S. Agneessens, H. Rogier, and M. Bozzi, Wearable textile antenna in substrate integrated waveguide technology, Electron. Lett., (2012), 48(16): 985-987.

[13] T. Kaufmann, Z. Xu, and C. Fumeaux, Wearable substrate-integrated waveguide with embroidered vias, The 8th European Conference on Antennas and Propagation (EuCAP), (2014), 1746-1750.

[14] S. Lemey and H. Rogier, SIW textile antennas as a novel technology for UWB RFID tags, 2014 IEEE RFID Technology and Application Conference (RFID-TA), (2014), 256-260.

[15] R. Moro, S. Agneessens, H. Rogier, Arnaut Dierck, and Maurizio Bozzi, Textile microwave components in substrate integrated waveguide technology, IEEE Trans. Microw. Theory Tech., (2015), 63(2): 422-432.

[16] M. Mackowiak, C. Oliveira, C. Lopes, and L. M. Correia, A statistical analysis of the influence of the human body on the radiation pattern of wearable antennas, 2011 IEEE 22nd International Symposium on Personal, Indoor and Mobile Radio Communications, (2011), 2214-2218.

[17] T. S. P. See and Z. N. Chen, Effects of human body on performance of wearable PIFAs and RF transmission, Antennas and Propagation Society International Symposium, (2005), 686-689.